JOURNAL OF CATALYSIS 125, 554–564 (1990)

Influence of Thorium on the Surface Structure and CO Hydrogenation Activity of Silica-Supported Nickel Catalysts

JEFFREY S. LEDFORD, MARWAN HOUALLA, ANDREW PROCTOR, AND DAVID M. HERCULES

Department of Chemistry, University of Pittsburgh, Pittsburgh, Pennsylvania 15260

Received December 28, 1989; revised April 27, 1990

X-ray photoelectron spectroscopy (ESCA or XPS), ion scattering spectroscopy (ISS), X-ray diffraction (XRD), H_2 chemisorption, and gravimetric analysis have been used to characterize a series of Ni/Th/SiO_2 catalysts. The information obtained from surface and bulk techniques has been compared with CO hydrogenation activity and selectivity of the supported nickel catalysts. Comparison of measured ESCA Th/Si intensity ratios with values predicted by a theoretical model shows that the particle size of the Th phase increases from 1.4 to 4.2 nm as the Th/Si atomic ratio increases from 0.0036 to 0.023. ESCA and XRD results also indicate that nickel is present as poorly dispersed NiO on the calcined unpromoted catalyst. Reducibility of the Ni phase in all catalysts exceeds 97%. ESCA data show that Th addition has little effect on Ni metal dispersion up to a Th/Si atomic ratio of 0.015. For higher Th loadings, the Ni dispersion increases from approximately 6 to 9% with increasing Th loading. H_2 chemisorption data suggest that Ni dispersion increases from 4.8 to 9.8% with increasing Th content. The turnover frequency (TOF) for CO hydrogenation calculated using ESCA estimates of Ni dispersion increases by a factor of 9 as the Th/Si atomic ratio increases from 0 to 0.015. For higher Th loadings the TOF decreases, but it remains seven times the value observed for the unpromoted catalyst. These results have been explained in terms of the Th surface coverage indicated by ISS. Th addition also increases olefin selectivity and the yield for higher hydrocarbons.

INTRODUCTION

The influence of promoters on the catalytic activity of supported metal catalysts has led to many studies devoted to a better understanding of the way additives affect the reactivity of the active phase. Praliaud *et al.* (*1*) reported that addition of potassium to a Ni/SiO_2 catalyst decreases CO hydrogenation activity and increases the selectivity to olefinic products. This effect was attributed to an increase in electron density of the nickel phase which increased the strength of the Ni–CO bond and decreased the Ni–H bond strength. Ryndin *et al.* (*2*) reported that Ti promotion of a Ni/SiO_2 catalyst increased the CO hydrogenation activity and selectivity to C2 and C3 hydrocarbons. In this case, promotion of the catalytic properties was attributed to interaction between dispersed nickel metal paticles and low-valent titanium ions.

The use of actinide promoters in Group VIII metal-based methanation catalysts to increase activity and improve selectivity to higher hydrocarbons is well known (*3–10*). Hadjigeorghiou and Richardson (*9*) reported that ThO_2 promotion of coprecipitated NiO/ThO_2 catalysts increases CO hydrogenation activity by accelerating the dehydration rate of an enolic species at the Ni–ThO_2 interface. Kip *et al.* (*10*) attributed increased activity of a Th-promoted Rh/SiO_2 catalyst to formation of "side-bonded" CO which has a lower C–O bond strength and thus a higher dissociation rate than other adsorbed CO species.

Much of the previous research on the effects of actinide promoters has focused on catalytic properties of the promoted cata-

0021-9517/90 $3.00

lysts. Little effort has been devoted to systematically investigating the relationship between surface structure and catalytic activity. The present work is part of a broad study to investigate the structure and reactivity of rare earth and actinide-promoted Group VIII metal-based CO hydrogenation catalysts. In this paper, X-ray photoelectron spectroscopy (XPS, ESCA), ion-scattering spectroscopy (ISS), X-ray diffraction (XRD), gravimetric analysis, and H_2 chemisorption are used to examine the state and dispersion of nickel and thorium supported on silica. The information derived from spectroscopic measurements is compared with CO hydrogenation activity to evaluate the influence of thorium promotion on the activity and selectivity of supported nickel catalysts.

EXPERIMENTAL

Catalyst preparation. Nickel–thorium catalysts were supported on aerosil silica (Degussa; surface area: 225 m^2/g) which had been wetted with deionized water, calcined for 24 h at 500°C, and ground. Since silica is known to rehydroxylate slowly (*11*), the support used to prepare these catalysts may be partially dehydroxylated. Catalysts prepared on fully hydroxylated SiO_2 resulted in a higher Ni dispersion, but the effect of Th was similar to that reported in this study (*12*).

Catalysts were prepared by coimpregnation to incipient wetness with solutions of nickel and thorium nitrates (Fisher purified). The pH of the impregnating solutions decreased from 3 to 0.5 with increasing Th concentration. The catalysts were dried for 12 h at 110°C and calcined for 12 h at 400°C. The nickel content was constant for all samples and equal to 3 wt% of the unmodified support; the thorium content was varied to produce Th/Si atomic ratios from 0 to 0.031 (0 to 11.6 wt% ThO_2). Catalyst samples will be designated as NiThy, where y is the Th/Si atomic ratio ($\times 10^2$). Increasing the thorium content of the catalysts decreases the BET surface area by a maximum of 15%.

Standard materials. NiO was prepared by calcining nickel nitrate (Fisher purified) at 800°C for 8 h. ThO_2 was prepared by calcination of a carbonate precipitate of the nitrate salt at 350°C for 24 h. XRD patterns of the standard compounds matched the appropriate ASTM powder diffraction files.

X-ray diffraction. X-ray powder diffraction patterns were obtained using a Diano XRD-6 diffractometer employing Ni-filtered Cu$K\alpha$ radiation (1.54056 Å). The X-ray tube was operated at 50 kV and 25 mA. Catalysts were run as pellets mounted on a glass slide. Spectra were scanned at a rate of 0.4° min^{-1} (in 2θ).

The mean crystallite sizes ($\bar{d}$) of NiO and ThO_2 particles were determined from XRD line broadening measurements using the Scherrer equation (*13*),

$$\bar{d} = K\lambda/\beta \cos\theta, \qquad (1)$$

where λ is the X-ray wavelength, K is the particle shape factor, taken as 0.9, and β is the full width at half maximum (fwhm), in radiáns, of the NiO ⟨111⟩ or ThO_2 ⟨111⟩ line. Reported crystallite sizes were corrected for instrumental broadening as described by Klug and Alexander (*13*).

The absolute intensity of the NiO diffraction peak measured for the NiThy catalysts decreased by 75% as the Th content increased from 0 to 0.031. A similar decrease (80%) in NiO intensity was observed for a calcined 3 wt% Ni/SiO_2 catalyst following impregnation of the catalyst with a buffered (pH 4) thorium nitrate solution chosen to give a Th/Si atomic ratio of 0.031. Since it is unlikely that impregnation with a buffered Th nitrate solution will disrupt the NiO crystal structure, we conclude that Th addition decreases the intensity of the Cu$K\alpha$ radiation diffracted from NiO. Indeed, thorium has a high absorption coefficient for X-ray radiation with a wavelength comparable to the Cu$K\alpha$ (*14*). Thus, absolute intensities of the NiO XRD peaks cannot be used for quantitative analysis of the catalysts.

ESCA spectra. ESCA spectra were obtained using a Leybold–Heraeus LHS-10

electron spectrometer equipped with an aluminum anode (1486.6 eV) operated at 240 W (12 kV, 20 mA). The spectrometer was interfaced to an LH-DS5XS data system which utilized an HP1000 computer to process digital data. The operating pressure was typically below 1×10^{-8} Torr in the analysis chamber. Reduced catalysts were prepared in a reactor attached to the spectrometer and transferred directly to the analysis chamber without exposure to air (*15*). Reduction was carried out by flowing H_2 (100 cm^2 min^{-1}, 99.999%) over the catalysts for 12 h. The Si 2*p* line from the support was used as the binding energy reference for the catalysts (103.5 eV). The binding energies measured for standard compounds were referenced to the C 1*s* line (284.6 eV) of the carbon overlayer. ESCA binding energies were measured with a precision of ±0.2 eV, or better.

Quantitative ESCA analysis. It has been shown by Defosse *et al.* (*16*) that one can calculate the theoretical intensity ratio (I_m^0/I_s^0) expected for a supported phase (m) atomically dispersed on a carrier (s). An extension of the Defosse model proposed by Kerkhof and Moulijn (*17*) has been used in the present investigation. The photoelectron cross-sections and the mean escape depths of the photoelectrons used in these calculations are taken from Scofield (*18*) and Penn (*19*), respectively. The escape depth used for thorium (1.7 nm) was calculated for the Th $4f_{7/2}$ photoelectron using expressions taken from Penn (*19*).

For a phase (m) present as discrete particles, the experimental intensity (I_m/I_s) is given by the expression

$$I_m/I_s = I_m^0/I_s^0\,[1 - \exp(-d/\lambda_m)]/d/\lambda_m, \quad (2)$$

where d is the length of the edge of the cubic crystallites of the deposited phase and λ_m is the mean escape depth of the photoelectrons in (m). Dispersion of nickel metal is calculated from the edge length, d, by assuming that five sides of the cubic particle are exposed and that the area of a nickel metal atom is 0.0633 nm^2 (*20*).

Ion-scattering spectra. ISS spectra were obtained with a Leybold–Heraeus LHS-10 surface analysis system which uses an EA-10 hemispherical analyzer to measure the energy of the backscattered ions. Monoenergetic $^4He^+$ ions were used with a primary ion energy of 1500 eV. A base pressure of 1×10^{-8} Torr was obtained in the ion gun before rare gas was admitted. Spectra were obtained with a helium pressure of 2×10^{-5} Torr in the gun. This results in a current density of approximately 200 nA/cm^2. The laboratory scattering angle is 120°. Catalysts were run as pressed pellets.

Gravimetric analysis. Gravimetric analysis of the catalysts was carried out using a Cahn 113 microbalance. Approximately 100 mg of catalyst was dried for 4 h at 435°C in a flow of 10% O_2/He (99.999%) prior to reduction. Reduction was carried out at 400°C for 12 h in a flow of H_2 (99.999%). Samples were reoxidized for 4 h at 435°C in a flow of 10% O_2/He (99.999%). The extent of nickel reduction was calculated from the weight change that occurred on reoxidation.

Hydrogen chemisorption. Hydrogen chemisorption was performed in a conventional stainless-steel volumetric system evacuated by mechanical and oil diffusion pumps. The base pressure of the system was approximately 5×10^{-6} Torr. A MKS-390 Baratron pressure transducer was used for pressure measurements over a range of 0 to 1000 Torr. Following reduction in H_2 (99.999%) for 12 h at 400°C, the samples were evacuated for 1 h at the reduction temperature. Following evacuation, the samples were cooled to 25°C to perform the adsorption experiment. H_2 uptakes were measured by the adsorption (increasing pressure) method. The total gas uptake was calculated by extrapolating the linear portion of the adsorption isotherm to 0 Torr. The number of exposed Ni atoms was determined from the total H_2 uptake (H/Ni = 1). Nickel metal dispersion is defined as the ratio of exposed nickel atoms to the total number of Ni atoms.

Catalytic activity. Measurement of CO hydrogenation activity was performed in a

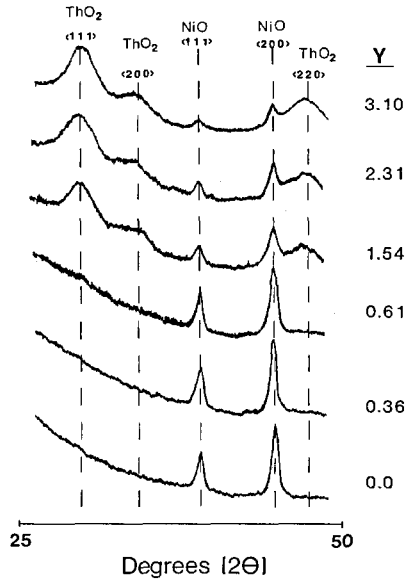

FIG. 1. X-ray diffraction patterns of NiThy catalysts, y = Th/Si atomic ratio ($\times 10^2$).

flow microreactor with a 25 cm^3 min^{-1} flow of H_2/CO/He (9/3/88%) at 185°C. Reactant gas flow rates were held constant with Matheson mass flow controllers and reactor temperatures were fixed using Honeywell DC100 controllers. Product gases were passed through a heated transfer line to a Perkin–Elmer Sigma 2000 gas chromatograph. Hydrocarbons were separated on a 6-m packed column containing Chromosorb 102. Olefin/paraffin separation was achieved using a 6-m packed column containing VZ-10. The chromatograph was interfaced to a Perkin–Elmer LCI-100 integrator for data analysis. The CO hydrogenation activity decreases approximately 50% during the first 10 h of reaction. Thus, activity data are reported for catalysts that have been on stream for 10 to 30 h. The conversion was less than 5% at steady state. Selectivities are reported for catalysts operated at similar conversions.

RESULTS

State and Dispersion of Thorium

X-ray diffraction analysis of catalysts with Th/Si atomic ratios ≥0.015 (≥6.1 wt% ThO_2) showed peaks characteristic of ThO_2 (Fig. 1). ESCA Th $4f_{7/2}$ binding energies measured for *in situ* oxidized and reduced catalysts are given in Table 1. The Th $4f_{7/2}$ binding energies measured for oxidized and reduced catalysts decreased from 335.5 to 334.8 eV with increasing Th content. The Th $4f_{7/2}$ binding energies measured for NiThy catalysts are higher than the value measured for ThO_2 (333.6 eV).

Figure 2 shows the variation in the Th $4f_{7/2}$/Si $2p$ intensity ratio measured for the calcined NiThy catalysts as a function of Th/Si atomic ratio (open circles). The Th/Si intensity ratios measured for reduced NiThy catalysts (solid circles) are identical, within experimental error, to the values measured for the calcined catalysts. The theoretical line calculated for monolayer dispersion is shown for comparison. The Th/Si intensity ratios measured for the catalysts are lower than the values predicted for monolayer dispersion. Variation in the particle size of the thorium phase calculated from ESCA intensity ratios using Eq. (1) is given as a function of the Th/Si atomic ratio in Table 2. Particle sizes determined from X-ray diffraction line broadening calculations using the ThO_2 ⟨111⟩ peak are also given for comparison. The mean particle size of the Th phase calculated from ESCA intensity ratios increases from 1.4 to 4.2 nm as the Th/Si atomic ratio increases from 0.0036 to 0.023. For catalysts with Th/Si atomic ratios ≥0.015, XRD line broadening calculations

TABLE 1

Th $4f_{7/2}$ Binding Energies Measured for Calcined and Reduced Catalysts

Th/Si atomic ratio ($\times 10^2$)	Binding energies (eV)	
	Oxidized	Reduced
0.36	335.5	335.5
0.61	335.4	335.5
1.54	335.1	335.1
2.31	334.8	334.9
3.10	334.9	334.8
ThO_2	333.6	

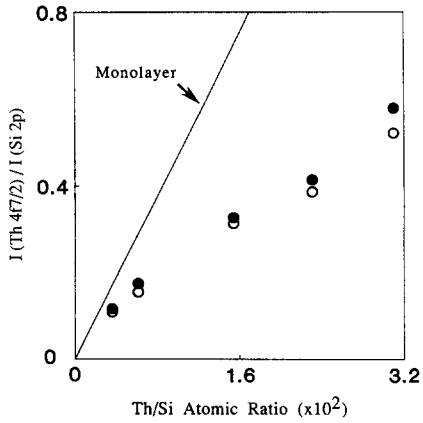

FIG. 2. ESCA Th $4f_{7/2}$/Si $2p$ intensity ratio of calcined (○) and reduced (●) NiThy catalysts plotted as a function of Th/Si atomic ratio. Th $4f_{7/2}$/Si $2p$ intensity ratios calculated for monolayer dispersion (—).

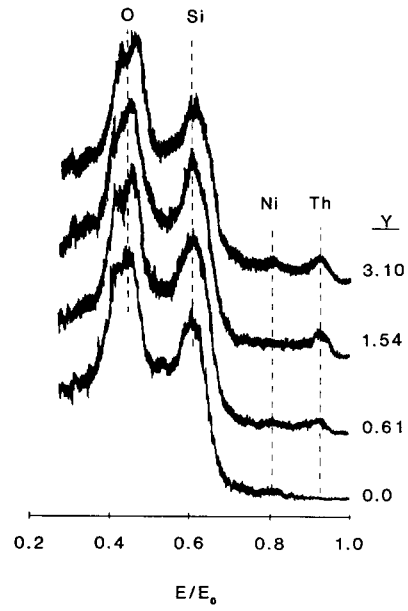

FIG. 3. ISS spectra measured for selected NiThy catalysts, y = Th/Si atomic ratio ($\times 10^2$).

show that the ThO_2 particle size is approximately 3.1 ± 0.3 nm and does not vary significantly with Th loading.

ISS spectra measured for several NiThy catalysts are shown in Fig. 3. Variation in the Th/Si ISS intensity ratio versus Th/Si atomic ratio for calcined (open circles) and reduced (solid circles) NiThy catalysts is given in Fig. 4. The ISS Th/Si ratio increases with increasing Th loading up to a Th/Si atomic ratio of 0.015 (6.1 wt% ThO_2) and levels off for higher Th loadings.

State and Dispersion of Nickel

X-ray diffraction analysis of the calcined catalysts shows lines characteristic of NiO for all catalysts (Fig. 1). The ESCA Ni $2p_{3/2}$ binding energies measured for the calcined catalysts (855.9 ± 0.1 eV) are independent of Th loading and higher than the value measured for NiO (853.9 eV). We must note that the Ni $2p_{3/2}$ peaks measured for NiThy catalysts are broad and featureless (FWHM = 5.5 eV) and thus the main peak and shake-up satellite that is commonly observed for

TABLE 2

Comparison of Thorium Particle Sizes Calculated for Calcined Catalysts Using ESCA Intensity Ratios and XRD Line-Broadening Calculations

Th/Si atomic ratio ($\times 10^2$)	Particle size (nm)	
	ESCA	XRD
0.36	1.4	—[a]
0.61	2.0	—[a]
1.54	3.3	3.4
2.31	4.2	2.9
3.10	4.1	3.0

[a] No ThO_2 XRD peaks detected for these catalysts.

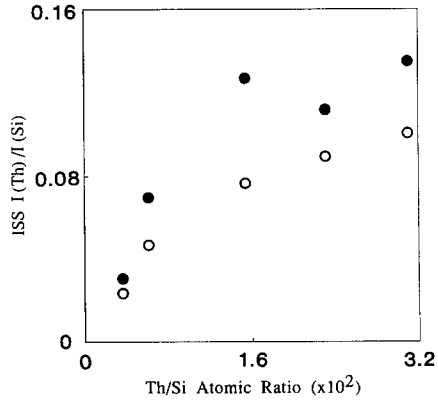

FIG. 4. ISS Th/Si intensity ratio of calcined (○) and reduced (●) NiThy catalysts plotted as a function of Th/Si atomic ratio.

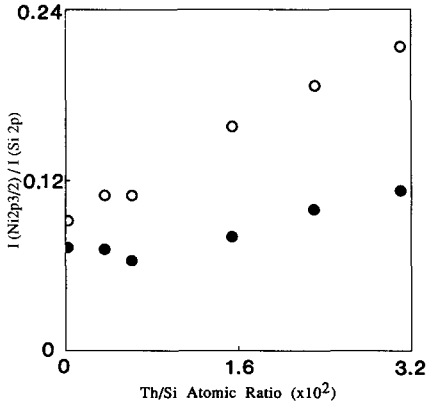

FIG. 5. ESCA Ni $2p_{3/2}$/Si $2p$ intensity ratio of calcined (○) and reduced (●) NiThy catalysts plotted as a function of Th/Si atomic ratio. Monolayer value = 1.42.

NiO (853.9 and 855.4 eV, respectively (*21*) cannot be resolved. Thus, the high binding energies reported for the calcined catalysts can be attributed, in part, to the poor resolution of the spectra collected for the calcined catalysts.

Variation in the Ni $2p_{3/2}$/Si $2p$ intensity ratio measured for the calcined catalysts is given as a function of Th/Si atomic ratio in Fig. 5 (open circles). The theoretical value for monolayer dispersion is 1.42. The measured intensity ratios increase from approximately 0.09 to 0.21 as the Th/Si atomic ratio increases from 0 to 0.031. Table 3 shows the nickel particle size calculated for calcined catalysts using both ESCA intensity ratios and XRD line broadening measurements. Assuming that Ni is present as NiO in the calcined catalysts, it can be seen that NiO particle sizes calculated from ESCA intensity ratios decrease from 16.1 to 6.9 nm with increasing Th content. For catalysts with Th/Si atomic ratios <0.015 (<6.1 wt% ThO_2), the NiO particle sizes determined from X-ray diffraction line broadening calculations are approximately 24.7 nm. For NiThy catalysts with higher Th loadings, the particle sizes calculated from XRD peak widths must be considered as approximations due to the low intensity of the NiO ⟨111⟩ peak (see Experimental).

TABLE 3

Comparison of Nickel Oxide Particle Sizes Calculated for Calcined Catalysts Using ESCA Intensity Ratios and XRD Line Broadening Measurements

Th/Si atomic ratio (×10²)	Particle size (nm)	
	ESCA	XRD
0.0	16.1	25.4
0.36	13.6	23.3
0.61	13.6	25.4
1.54	9.5	(16.5)[a]
2.31	8.0	(20.5)[a]
3.10	6.9	(16.7)[a]

[a] Values for these catalysts should be considered as estimates due to low intensity of the NiO peak.

ESCA spectra of the Ni $2p_{3/2}$ level measured for reduced catalysts showed one main peak at 852.6 ± 0.3 eV, characteristic of nickel metal. Weak features due to the metal plasmon (~858.9 eV) and nickel oxide are also observed in the spectra measured for the reduced catalysts. The extent of Ni reduction can be calculated by assuming that the unreduced fraction of nickel oxide is present as a Ni–SiO_2 surface phase (*22*). Table 4 shows the variation in Ni reducibility determined from ESCA and gravimetric data. It can be seen that the Ni phase is extensively reduced (97–100%). Variation

TABLE 4

Influence of Thorium Content on Nickel Reducibility Determined from ESCA and Gravimetric Data

Th/Si atomic ratio (×10²)	Percent reduction	
	ESCA	Gravimetric
0.0	99	100
0.36	99	—[a]
0.61	99	—[a]
1.54	98	97
2.31	97	—[a]
3.10	97	98

[a] Gravimetric analysis not performed for these catalysts.

TABLE 5

Influence of Thorium Content on Nickel Particle Size[a] and Nickel Dispersion Calculated from ESCA and H_2 Chemisorption Data

Th/Si atomic ratio ($\times 10^2$)	Particle size (nm)	Percent dispersion	
		ESCA	Chemisorption
0.0	20.6	6.0	4.8
0.36	20.6	6.0	4.7
0.61	23.3	5.3	4.8
1.54	18.4	6.7	7.1
2.31	15.0	8.1	8.4
3.10	13.1	9.2	9.8

[a] Calculated from ESCA data.

in the Ni $2p_{3/2}$/Si $2p$ intensity ratio measured for reduced catalysts is also given as a function of Th/Si atomic ratio in Fig. 5 (closed circles). For catalysts with Th/Si atomic ratios ≤ 0.015, Th addition has little effect on the Ni/Si intensity ratios. For Th-rich catalysts, the Ni/Si intensity ratios increase from approximately 0.07 to 0.11 with increasing Th content. Variations in the nickel metal dispersion determined from ESCA intensity ratios and H_2 chemisorption data are given in Table 5 as a function of Th/Si atomic ratio. Nickel metal particle sizes calculated from ESCA intensity ratios are also given in Table 5. One can see that for catalysts with Th/Si atomic ratios ≤ 0.015, Th addition has little effect on the Ni metal dispersion (~6%) calculated from ESCA data. For higher Th loadings, the Ni dispersion increases from approximately 6 to 9% with increasing Th content. The Ni dispersions values calculated from H_2 chemisorption data agree with those derived from ESCA. For both oxidized and reduced catalysts, the Ni ISS intensities were too small to be accurately measured.

CO Hydrogenation Activity and Selectivity

Variation in the CO hydrogenation rate measured per gram nickel metal is given as a function of Th/Si atomic ratio of the catalysts in Fig. 6. Addition of Th up to a Th/Si atomic ratio of 0.015 (6.1 wt% ThO_2) increases the rate for CO hydrogenation by nearly a factor of 10. Further additions of Th up to a Th/Si atomic ratio of 0.031 have little effect on the rate. Variation in the TOF for CO hydrogenation calculated from H_2 chemisorption (solid circles) and ESCA (open circles) estimates of nickel metal dispersion is given as a function of Th/Si atomic ratio in Fig. 7. The TOF for CO hydrogenation determined using ESCA estimates of Ni metal dispersion increases by a factor of 9 as the Th/Si atomic ratio increases from 0 to 0.015. Further additions of Th decrease the TOF, but the values remain seven times the TOF measured for the un-

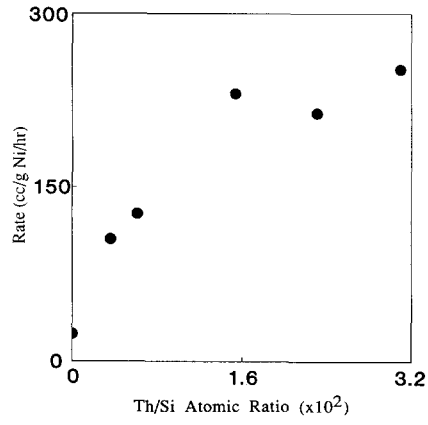

FIG. 6. Rates (cc/g Ni/h) measured for CO hydrogenation as a function of Th/Si atomic ratio.

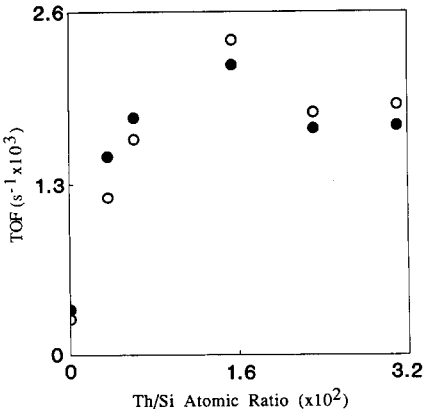

FIG. 7. Turnover frequency (TOF) measured for CO hydrogenation using ESCA (○) and H_2 chemisorption (●) estimates of Ni metal dispersion as a function of Th/Si atomic ratio.

promoted catalyst. The variation in TOF as a function of Th loading calculated from H_2 chemisorption estimates of Ni dispersion shows a trend similar to that calculated using ESCA data.

Variation in the weight fraction of methane and higher hydrocarbons produced by the catalysts and the olefin/paraffin ratio are given as a function of Th/Si atomic ratio in Table 6. The methane fraction produced by the catalysts decreases from 62 to 26 wt% for the lowest amount of Th promotion studied (Th/Si = 0.0036). Further additions of Th decrease the methane yield to approximately 18%. The selectivity to olefins is also significantly enhanced with the lowest addition of thorium. As shown in Table 6, the selectivity to olefinic products measured for the NiTh0.36 catalyst is over three times the value measured for the unpromoted catalyst. Further additions of Th increase the olefin/paraffin ratio to a value approximately four times that measured for the unpromoted catalyst.

DISCUSSION

Chemical State and Dispersion of Thorium

For catalysts with Th/Si atomic ratios ≤0.0061 (≤2.5 wt% ThO_2), the mean particle size of the Th phase (≤2.0 nm) calculated from ESCA data indicates that Th is well-dispersed over the silica carrier. This is consistent with XRD results which do not show the presence of crystalline Th compounds (Fig. 1). The dispersed Th phase can be attributed to the formation of small ThO_2 particles or to the presence of a mixture of Th–SiO_2 surface interaction species and ThO_2 particles. The high Th $4f_{7/2}$ binding energy shift observed for catalysts with low Th loadings (Table 1) is in accord with the presence of a Th–SiO_2 surface phase. This is consistent with the results of Zaki and Kolta (*23*) which indicate that approximately 0.095 mmol Th^{4+} ions/g SiO_2 will adsorb onto a high-surface-area (640 m^2/g) silica gel from acidic (pH < 3) nitrate solution by ion exchange. This corresponds to a Th/Si atomic ratio of 0.002 after normaliza-

TABLE 6

Influence of Thorium Content on the Selectivity to Higher Hydrocarbons and Olefins

Th/Si atomic ratio (× 10^2)	Hydrocarbon yield (wt%)					Olefin/paraffin yield (wt%)
	C1	C2	C3	C4	C5+	
0.0	62	11	14	6	7	0.8
0.36	26	10	20	14	30	2.5
0.61	20	7	16	17	40	3.0
1.54	16	6	17	19	42	3.7
2.31	19	7	16	13	45	3.2
3.10	16	8	17	17	42	3.8

tion for the surface area of the SiO_2 used in our study.

For catalysts with Th/Si atomic ratios ≤ 0.023, ESCA data show that the mean particle size of the thorium phase increases with increasing Th loading (Table 2). The increase in Th particle size can be attributed to an increase in the fraction of Th present as ThO_2 crystallites in the catalysts. This is consistent with the decrease in Th $4f_{7/2}$ binding energies measured for Th-rich catalysts.

Chemical State and Dispersion of Nickel

XRD results indicate that large particles (~25.4 nm) of NiO are formed on the unpromoted Ni/SiO_2 catalyst. This is consistent with the low ESCA Ni/Si intensity ratio measured for the catalyst and the large nickel particle size (16.1 nm) calculated using Eq. (1) (Table 3). The formation of large NiO aggregates on SiO_2-supported catalysts, prepared by incipient wetness, is well known (*24*). Ni^{2+} ions adsorbed from nitrate solutions are weakly held by the carrier (*25*). Thus, during drying and calcination, adsorbed Ni species migrate over the SiO_2 surface and form large NiO aggregates.

The difference in NiO particle size calculated from XRD line broadening and ESCA Ni/Si intensity ratios may be understood in terms of the limitations of X-ray diffraction. It is well known that particle sizes determined from XRD line broadening calculations are skewed to large values since highly dispersed particles ($d < 3.0$ nm) will not be detected by XRD. Thus, we attribute the smaller NiO particle size calculated from ESCA intensity ratios to the presence of small particles that are not detected by XRD.

NiO particle sizes calculated from ESCA Ni/Si intensity ratios (Table 3) indicate that Th addition decreases the mean NiO particle size. This suggests that the ThO_2 phase can act as a "spacer" on the silica carrier, inhibiting migration of the nickel during calcination.

The decrease in ESCA Ni/Si intensity ratios following reduction (Fig. 5) indicates that reduction decreases the dispersion of the Ni phase. The variation in Ni/Si intensity ratios as a function of Th/Si atomic ratio shows that Th addition increases the Ni dispersion, but to a lesser extent than that observed for oxidic catalysts.

Influence of Thorium on CO Hydrogenation Activity

The TOF for CO hydrogenation calculated from H_2 chemisorption and ESCA estimates of Ni metal dispersion increases by approximately a factor of 8 as the Th/Si atomic ratio increases from 0 to 0.015 (Fig. 7). Further additions of thorium decrease slightly the TOF for CO hydrogenation. Note that the variation in TOF is similar to the variation in Th/Si ISS intensity ratio measured for the reduced catalysts (Fig. 4). This suggests that the promotion effect of Th is related to the Th surface coverage on the catalysts. Since ISS has a higher surface sensitivity than ESCA (approximately 2 versus 20 Å), we expect the ISS Th/Si intensity ratios to more accurately reflect the Th surface coverage.

One explanation for this effect is that Th promotion of the Ni/SiO_2 catalyst involves formation of active sites by Th decoration of the Ni metal particles. This is consistent with results reported by Kip *et al.* (*10*) for the effect of ThO_2 promotion on the CO hydrogenation activity of Rh/SiO_2 catalysts. These authors concluded from IR measurements that ThO_2 promotion involved the formation of "side-bonded" CO which had a lower C–O bond strength and thus a higher dissociation rate than linearly bonded CO. Similar mechanisms have been proposed by Burch *et al.* (*26, 27*) for TiO_2-supported Ni, Pd, and Ir catalysts; Rieck and Bell (*28, 29*) for Pd/La_2O_3 catalysts; and Sachtler *et al.* (*30, 31*) for Mn- or Mn–Mo-promoted Rh/SiO_2 catalysts. The promotion mechanism involves the activation of adsorbed CO by the interaction of a promoter ion with the oxygen atom of a chemisorbed carbonyl. The ions of the promoter on the surface of

the metal provide sites at which the carbon monoxide is bonded with its carbon atom to the metal atom and its oxygen atom to the promoter ion. This results in formation of "side-bonded" CO.

Th addition to the Ni/SiO_2 catalysts also dramatically increases the selectivity to higher hydrocarbons and olefins. These results may also be explained by the presence of Th-promoted Ni sites on the surface of the Ni metal particles. In principle, an increase in the amount of active carbon on the catalyst surface will increase the ratio of active carbon to hydrogen. This would decrease the rate of chain-terminating steps responsible for the production of lighter hydrocarbons. In addition, the rate of secondary hydrogenation reactions that produce paraffins from adsorbed alkene intermediates would be lower on a catalyst surface that had a higher active carbon/hydrogen ratio. Hadjigeorhiou and Richardson (*9*) also reported that ThO_2 promotion of a Ni catalyst increased the selectivity to higher hydrocarbons. However, the authors have attributed the increased selectivity to an increase in the amount of $[CH]_{ads}$ relative to $[CH_2]_{ads}$ at the ThO_2–Ni interface.

CONCLUSIONS

The combined use of several techniques to investigate the effect of Th addition on the structure and CO hydrogenation activity of Ni/SiO_2 catalysts leads to the following conclusions.

(1) ESCA data indicate that for low Th loadings (Th/Si <0.015), Th is present as a Th–SiO_2 surface phase. For higher Th loadings, the fraction of Th present as ThO_2 crystallites increases with Th loading.

(2) ESCA and XRD data show that the unpromoted Ni/SiO_2 catalyst contains large NiO particles (~16 nm). ESCA data show that Th addition increases the dispersion of the oxidic nickel phase. ESCA and H_2 chemisorption data indicate that Th addition also increases the Ni metal dispersion. These results have been attributed to the presence of ThO_2 which acts as a spacer inhibiting agglomerate formation on calcination.

(3) Thorium addition up to a Th/Si atomic ratio of 0.015 (6.1 wt% ThO_2) increases the TOF for CO hydrogenation by a factor of 8. Further additions of Th decrease slightly the TOF. The selectivity to higher hydrocarbons and olefins is significantly increased by Th promotion. These results have been correlated with the Th surface coverage determined by ISS.

ACKNOWLEDGMENTS

This work was supported by the National Science Foundation under Grants CHE-8411835 and CHE-8401202. JSL acknowledges the A. W. Mellon Educational and Charitable Trust for a predoctoral fellowship.

REFERENCES

1. Praliaud, H., Dalmon, J. A., Mirodatos, C., and Martin, G. A., *J. Catal.* **97,** 344 (1986).
2. Ryndin, Y. A., Alekseev, O. S., Vasileva, M. N., Zaikovskii, V. I., and Ermakov, Y.I., *Kinet. Katal.* **28**(4), 900 (1987).
3. Fischer, F., and Meyer, K., *Brennst. Chem.* **12,** 225 (1931).
4. Pichler, H., and Ziesecke, K. H., *Brennst. Chem.* **30,** 13 (1949).
5. Rao, V. U. S., Gormley, R. J., Shamsi, A., Petrick, T. R., Stencel, J. M., Schehl, R. R., and Chi, R. D. H., *J. Mol. Catal.* **29,** 271 (1985).
6. Denise, B., and Sneeden, R. P. A., *React. Kinet. Catal. Lett.* **26,** 265 (1987).
7. Turlier, P., and Martin, G. A., *React. Kinet. Catal. Lett.* **25,** 1 (1984).
8. Hadjigeorghiou, G. A., and Richardson, J. T., *Appl. Catal.* **21,** 37 (1986).
9. Hadjigeorghiou, G. A., and Richardson, J. T., *Appl. Catal.* **21,** 47 (1986).
10. Kip, B. J., Hermans, E. G. F., Van Wolput, J. H. M. C., Hermans, N. M. A., Van Grondelle, J., and Prins, R., *Appl. Catal.* **35,** 109 (1987).
11. Mathias, J., and Wannemacher, G., *J. Colloid Interface Sci.* **125**(1), 61 (1988).
12. Ledford, J. S., Houalla, M., Kibby, C. L., Petrakis, L., and Hercules, D. M., *Stud. Surf. Sci. Catal.* **19,** 235 (1984).
13. Klug, H. P., and Alexander, L. E., *X-Ray Diffraction Procedures for Polycrystalline and Amorphous Materials,* 1st ed. Wiley, New York, 1954.
14. Clark, G. L., "The Encyclopedia of X-rays and Gamma Rays." Reinhold, New York, 1963.
15. Ledford, J. S., Hoffmann, D. P., Proctor, A., and Hercules, D. M., to be submitted.

16. Defosse, C., Canesson, P., Rouxhet, P. G., and Delmon, B., *J. Catal.* **51,** 269 (1978).
17. Kerkhof, F. P. J. M., and Moulijn, J. A., *J. Phys. Chem.* **83,** 1612 (1979).
18. Scofield, J. H., *J. Electron Spectrosc. Relat. Phenom.* **8,** 129 (1979).
19. Penn, D. R., *J. Electron Spectrosc. Relat. Phenom.* **9,** 29 (1976).
20. Coenen, J. W. E., Schats, W. M. T. M., and Van Meerten, R. Z. C., *Bull. Soc. Chim. Belg.* **88**(7,8), 435 (1979).
21. Kim, K. S., and Winograd, N., *Surf. Sci.* **43,** 625 (1974).
22. Stranick, M. A., Houalla, M., and Hercules, D. M., *J. Catal.* **103,** 151 (1987).
23. Zaki, M. R., and Kolta, K. B., *Indian J. Chem. Sect. A* **19,** 630 (1980).
24. Houalla, M., Delannay, F., Matsuura, I., and Delmon, B., *J. Chem. Soc. Faraday Trans. 1* **76,** 2128 (1980).
25. Anderson, J. H., *J. Catal.* **26,** 277 (1972).
26. Bracey, J. D., and Burch, R., *J. Catal.* **86,** 384 (1984).
27. Anderson, J. B. F., Bracey, J. D., and Burch, R., *in* "Proceedings, 8th International Congress on Catalysis, Berlin, 1984," Vol. V, pp. 111–121. Verlag Chemie, Weinheim, 1984.
28. Rieck, J. S., and Bell, A. T., *J. Catal.* **96,** 88 (1985).
29. Rieck, J. S., and Bell, A. T., *J. Catal.* **99,** 262 (1986).
30. Sachtler, W. M. H., *in* "Proceedings, 8th International Congress on Catalysis," Berlin, 1984, Vol. I, pp. 151–173. Verlag Chemie, Weinheim, 1984.
31. Van den Berg, F. G. A., Glezer, J. H. E., and Sachtler, W. M. H., *J. Catal.* **93,** 340 (1985).